KEK-77-3
May 1977

SYNCHRONOUS PHASE LAW EXPERIMENT IN THE KEK LINAC

Jiro TANAKA, Isamu SATO and Shigemi INAGAKI

National Laboratory for High Energy Physics
Oho-machi, Tsukuba-gun, Ibaraki-ken, 300-32, Japan

Hiroshi MATSUMOTO

Department of Physics, Faculty of Science, Nagoya University,
Chikusa-ku, Nagoya-shi, Japan

Shoji OKUMURA

Department of Information Science, Faculty of Engineering,
Fukui University
Bunkyo 3-9-1, Fukui-shi, Japan

NATIONAL LABORATORY FOR
HIGH ENERGY PHYSICS
OHO-MACHI, TSUKUBA-GUN
IBARAKI, JAPAN

KEK Reports are available from

Library
National Laboratory for High Energy Physics
Oho-machi, Tsukuba-gun
Ibaraki-ken, 300-32
JAPAN

Phone: 02986-4-1171
Telex: 3652-534 (Domestic)
(0)3652-534 (International)
Cable: KEKOHO

SYNCHRONOUS PHASE LAW EXPERIMENT IN THE KEK LINAC

Hiroshi MATSUMOTO*, Jiro TANAKA, Isamu SATO,
Shoji OKUMURA** and Shigemi INAGAKI

National Laboratory for High Energy Physics
Oho-machi, Tsukuba-gun, Ibaraki-ken, 300-32, Japan

Abstract

In the KEK 20 MeV linac, the electric field $\bar{E}$ increases linearly along the cavity from the injection end but the synchronous phase is supposed to be constant throughout the acceleration. While BNL group reported that the method of "synchronous phase law" reduced the energy spread and the variation in mean energy. The KEK linac consists of only single cavity, and the field distribution can be changed by fourteen tuners to some extent. So we tried the experiment of tilting the field distribution and varying the overall field level to find a better operating condition. However we could not find out any reason to operate at any other condition than our designed value in the aspect of the mean energy, the energy spread and the capture efficiency.

* Department of Physics, Faculty of Science, Nagoya University, Chikusa-ku, Nagoya-shi, Japan

** Department of Information Science, Faculty of Engineering, Fukui University, Bunkyo 3-9-1, Fukui-shi, Japan

1. Introduction

Since the first acceleration of 20 MeV proton beam on Aug.1, 1974 the KEK linac has been continuously improved and got a 150 mA beam at the end of '76. In the latest operation the energy spread is less than ±1.2 % without debuncher and ±0.3 % with debuncher at the peak current of 120 mA and the pulse length of 15 μs. Further, as the normalized emittance of 90 % intensity level is 0.6 π cm mrad at 120 mA, all the designed performances are attained.

In the U.S.-Japan seminar on high energy accelerator science held at Tokyo in 1974, G.W. Wheeler and L.C. Teng suggested to try an experiment of the "synchronous phase law" at KEK. In our design the axial mean field $\bar{E}$ is expressed as

$$\bar{E} = 1.5 + 0.04\,\ell \ (\mathrm{MV/m}), \tag{1}$$

where ℓ is the length from the low energy end to the gap center in meter. A constant synchronous phase $\phi_s = \cos^{-1} 0.9 = 25.8°$ is supposed throughout the 89 acceleration gaps. The linac has a single cavity and consists of six unit-tanks. The first and the last unit-tanks have three and the others two cylindrical tuners. They are used to vary the tilting of the field distribution. The method of calculation is reported in Ref.3.

"Synchronous phase law" can be described as follows.[1,2] The acceptance area A in most linacs is expressed by

$$A \propto \left[\frac{2\beta_s^3\gamma_s^3 e\bar{E}T\cos\phi_s}{m_0c^2} \right]^{1/2} \phi_s^{5/2} \tag{2}$$

where

$\beta_s c$ = synchronous velocity

$\gamma_s = (1 - \beta_s^2)^{-1/2}$

ϕ_s = synchronous phase (<0)

T = transit time factor

m_0 = proton mass

and Eq.1 states that varying ϕ_s as $(\beta_s\gamma_s)^{-3/5}$ will keep the acceptance from decreasing under the condition of constant synchronous acceleration $e\bar{E}T\cos\phi_s$ = const. A reduction of $|\phi_s|$ along the accelerating gaps will increase the maximum phase spread $\Delta\phi_{max}$ and reduce the maximum energy spread $\Delta\gamma_{max}$ compared to their values for constant ϕ_s as given by Eqs.3 and 4.

$$\Delta\phi_{max} \propto (\beta_s\gamma_s)^{-3/4} (\sin|\phi_s|)^{-1/4} \tag{3}$$

$$\Delta\gamma_{max} \propto (\beta_s\gamma_s)^{+3/4} (\sin|\phi_s|)^{+1/4}. \tag{4}$$

The effect of rf phase error α and amplitude error $\delta(=\delta E/E)$ on an initially synchronous particle can be given by the following equations.

$$\begin{aligned}\Delta\phi(s) = {} & k_\ell^{-1/2} (\beta_s\gamma_s)^{-3/2} \\ & \cdot[\sin(\int k_\ell ds)\int_0^s k_\ell^{3/2}(\beta_s\gamma_s)^{3/2} \cos(\int_0^{s'} k_\ell ds'')\cdot\{-\alpha(s')+\delta(s')\cot\phi_s\}ds' \\ & -\cos(\int k_\ell ds)\int_0^s k_\ell^{3/2}(\beta_s\gamma_s)^{3/2} \sin(\int_0^{s'} k_\ell ds'')\cdot\{-\alpha(s')+\delta(s')\cot\phi_s\}ds'],\end{aligned} \tag{5}$$

$$\begin{aligned}\Delta\gamma(s) = {} & -\lambda/(2\pi)\cdot k_\ell^{1/2}(\beta_s\gamma_s)^{3/2} \\ & \cdot[\cos(\int k_\ell ds)\int_0^s k_\ell^{3/2}(\beta_s\gamma_s)^{3/2} \cos(\int_0^{s'} k_\ell ds'')\{-\alpha(s')+\delta(s')\cot\phi_s\}ds' \\ & +\sin(\int k_\ell ds)\int_0^s k_\ell^{3/2}(\beta_s\gamma_s)^{3/2} \sin(\int_0^{s'} k_\ell ds'')\{-\alpha(s')+\delta(s')\cot\phi_s\}ds'],\end{aligned} \tag{6}$$

where λ is the wave length of the rf field and

$$k_\ell = [\frac{2\pi e\bar{E}T \sin|\phi_s|}{\lambda m_0c^2\beta_s^3\gamma_s^3}]^{1/2} .$$

Taking averages of the parameters in each tank, Batchelor et al got the expression for the mean square error of the final energy and concluded that an all over improvement in average energy can be expected for decreasing synchronous phase. Thereafter they got satisfactory results for the computer runs with the linear phase law, in which the synchronous phase is decreased linearly along the distance.

The design parameters for the KEK linac will be described in the next chapter, because they have not been put in order and will be used in the following calculations. The results of the bead perturbation measurement will be given in Chap.3. By the use of these data, the calcualtions of beam dynamics were executed and will be described in Chap.4. The experimental results will be shown in Chap.5.

2. Design Parameter

Originally the proton linac at KEK was intended as a 125 MeV injector for a 40 GeV proton synchrotron. The geometrical parameter of the 125 MeV linac is reported in Ref.4. The linac was designed to have five cavities with different inner diameter and to accelerate up to 10 MeV in the first tank and by 30 MeV in the every four tanks. When the 40 GeV proton synchrotron project was reduced to 8 GeV ones, the linac was also reduced to the present 20 MeV linac.

At that time we decided to make a single cavity because of its simplicity. The new dimensions of cells from No.1 to No.28 were determined by the data of a half model cavity, those from No.29 to No.56 by the data of MESSYMESH and those from No.57 to No.89 by the computer programme which was developed here using the method of M. Martini and D.J. Warner.[5)]

The field equation is given by

$$\frac{\partial^2 U}{\partial r^2} - \frac{1}{r}\frac{\partial U}{\partial r} + \frac{\partial^2 U}{\partial z} + k^2 U = 0 \qquad (7)$$

under the boundary condition of

$$\frac{\partial U}{\partial n} = 0 \ , \qquad (8)$$

where $U = rH_\phi$. We divide the region into $I(0 < r \leq r_D \equiv 2SD)$ and $II(r \geq r_D)$ (Fig.1). In the region II, U is approximated by the expansion

$$U = a_0 r F_1(kr) + \sum_{m=1}^{10} a_m r G_1(\gamma_n r) \cos\beta_m z, \tag{9}$$

where

$$F_1 = J_1(kr) - \frac{J_0(kD)}{Y_0(kD)} Y_1(kr) \ , \tag{10}$$

$$G_1 = I_1(\gamma_m r) + \frac{I_0(\gamma_m D)}{K_0(\gamma_m D)} K_1 \ (\gamma_m r) \tag{11}$$

and

$$\beta_m = 2\pi m/L, \qquad \gamma_m = \sqrt{\beta_m^2 - k^2} = \sqrt{\beta_m^2 - (\omega_0/c)^2}. \tag{12}$$

J_n and Y_n are Bessel functions of first and second kind and I_n and Kn are modified Bessel functions of first and second kind. The region I is divided by coarse mesh for $SD \leq r \leq 2SD$ and fine mesh for $0 < r \leq SD$. The values U on mesh point are calculated by the method of seuccessive over-relaxation. The expansion coefficients a_m in Eq.8 are determined by the continuity condition. Then the resonant frequency is calculated by the integration

$$k^2 = \frac{\int 1/r\{(\partial U/\partial r)^2 + (\partial U/\partial z)^2\}ds}{\int U^2/r \ ds} \ . \tag{13}$$

The iterations are continued until a desired accuracy is attained. The cell parameters such as the resonant frequencies, transit time factors, and rf losses were computed for a given cell length and different two gap lengths and those values at 201.25 MHz were determined by interpolation.

In order to reduce the discharges at the low energy side, the mean axial electric field is decided by Eq.1. The cell length L_n and velocity $\beta_{out}c$ for the n-th cell are

$$L_n = \frac{\bar{\beta}\lambda}{1 - \lambda/2\pi\cdot\bar{E}_n(1 - \beta_c^2)^{3/2}/m_0c^2\beta_c\cdot\bar{\beta}dT/d\beta_c\cdot\sin\phi_s} \tag{14}$$

$$\beta_{out} = \{1 - (m_0c^2)^2/(m_0c^2 + E_{in} + \bar{E}_nL_nT\ \cos\phi_s)^2\}^{1/2} \tag{15}$$

$$\bar{\beta} = (\beta_{in} + \beta_{out})/2 \tag{16}$$

where β_c is the value at the center of gap, approximated by $\bar{\beta}$ and $\bar{E}_n$ the axial mean field at n-th gap. The measured transit time factors by half model cavity were used for cells from 1 to 28. The gap distance and the drift tube length were determined as listed in Tables 1 and 2.

3. Field Distribution

The axial electric field in the cavity was measured by means of a bead perturbation method.[6)] The shift of frequency Δf due to a small metallic bead perturbation is given by

$$\Delta f/f = -3\varepsilon_0\ E^2V/4U \tag{17}$$

where f is the resonant frequency without the perturbation, ε_0 the free space dielectric constant, E the electric field at the position of the bead, V the volume of the bead and U the total stored energy in the cavity. The bead attached to a tensioned silk string was drived by a synchronous motor. The measured period of the beat (≈ 1 kHz) between a signal of constant frequency and the rf from the self excited cavity were transfered to and processed by a mini-computer OKITAC 4300. The average fields calculated for each gap were displayed on a storage-scope about 50 seconds after the bead started moving. The points in Fig.2 show the average axial electric field of the accelerating mode when the tuning was completed. The dashed straight line represents the design value Figs.3 and 4 shows the transit-time factor T_n and S-coefficient S_n defined by

$$T_n = \int E_z(z)\ \cos(k_nz)dz/\int E_z(z)dz \tag{18}$$

and

$$S_n = \int E_z(z)\ \sin(k_nz)dz/\int E_z(z)dz \tag{19}$$

respectively, where integrations are performed along the n-th gap length. After the evacuation of the linac tank, the field level along the cavity is relatively measured by the monitor loop probes supposing that the outputs are proportional to the axial electric field around them.

The tilt of the field is mainly adjusted by four tuners, two in the first and two in the last unit-tank. The deviation of the field ($\Delta E = E - E_n$) from the ideal normal mode value E_n can be written[7] as

$$\frac{1}{\bar{E}} \frac{d^2(\Delta E)}{dz^2} = (\Delta\gamma_p)^2 . \tag{20}$$

$\Delta\gamma_p$ is the local value of the propagation constant defined by

$$(\Delta\gamma_p)^2 = \frac{\omega_z^2}{c^2} - \frac{\omega^2}{c^2}(1 - \frac{i}{Q}) = \Gamma(-\frac{\delta\omega_z}{\omega} + \frac{i}{2Q}) , \tag{21}$$

$$\delta\omega_z = \omega - \omega_z,$$

where ω_z denotes the local frequency of the cavity, ω the driven frequency ω_T the resonant frequency of the entire cavity and $\Gamma \simeq 8\pi^2/\lambda^2 \times 1.2$ for drift tube loaded cavity. The linear increase in $\bar{E}$ is attained by the frequency perturbation in the first and last unit tank related by $\Delta\omega_i L_i = -\Delta\omega_f L_f$, where $\Delta\omega_z = \omega_z - \omega_T$ and L_z is the length of cavity with local frequency ω_z. The cavity was tuned by the insertion of the tuner and the frequency shift is given by

$$\frac{\Delta\omega}{\omega} = \frac{1}{4U}\int_{\delta v}(\mu_0 H^2 - \varepsilon_0 E^2)dV . \tag{22}$$

Fig.5 shows the measured field distribution for various tuner positions.

4. Computational Results of Motion

The equations of motion governing phase and radial motion are given by

$$\frac{d}{dn}[\gamma_s^3\beta_s^2 \frac{d}{dn}(\phi - \phi_s)] = -\frac{2\pi e E_0\lambda}{m_0 c^2} \varepsilon_s[I_0\cos\phi - \cos\phi_s] \tag{23}$$

and

$$\frac{\beta}{\beta_s}\frac{d}{dn}\left[\frac{\gamma\beta}{\beta_s}\frac{dr}{dn}\right] = \frac{-eE_0\lambda^2}{m_0c^2}\frac{I_1}{\sqrt{1-\beta_w^2}}(1-\beta\beta_w)\sin\phi \tag{24}$$

respectively, where n is rf cycles spent by the synchronous particle in traversing distance z and for a proton linac also the index number of the unit cell through which the bunch is instantaneously passing[8].

$$dz = v_s\, dt_s = \beta_s\lambda dn \tag{25}$$

If the argument of the Bessel function is small, above equations become

$$\frac{d}{dn}[\gamma_s^3\beta_s^2\frac{d}{dn}(\phi-\phi_s)] = -\frac{2\pi eE_0\lambda}{m_0c^2}\beta_s[\cos\phi-\cos\phi_s] \tag{26}$$

$$\frac{d}{dn}[\frac{\gamma\beta}{\beta_s}\frac{dr}{dn}] = -\frac{\pi eE_0\lambda}{m_0c^2\beta}(1-\beta\beta_s)r\sin\phi. \tag{27}$$

If we use the average field gradient $\bar{E}$ and transit time factor T, i.e.

$$\frac{dw_s}{dz} = eE_0(z)\cos\phi_s = e\bar{E}T\cos\phi_s, \tag{28}$$

the longitudinal motion Eq.26 can be rewritten as

$$\frac{d}{dn}[\gamma_s^3\beta_s^2\frac{d}{dn}(\phi-\phi_s)] + \frac{2\pi e\bar{E}T\lambda}{m_0c^2}\beta_s(\cos\phi-\cos\phi_s) = 0. \tag{29}$$

Though there are many papers[9] which take into account the space charge effect, we used Eq.29 in the following calculation.

Fig.6 shows the synchronous phase calculated using the measured average electric field and transit time factors given by Figs.2 and 3 for the cell and gap length in Table 1. As stated in Chap.2, different kind of data were used before and after the gap No.56 and there remained some mismatching. Fortunately the synchronous phase at Nos.57 and 58 are large, we are investigating to remodel four or six drift tubes.

A constant synchronous phase 25.8° is not maintained throughout the whole acceleration. Aside from the first drift tubes, ϕ_s changes from about 40° to 27.5° gradually in the first unit-tank (D/T No.1 ∿ No.28). However in the second and in the middle of the third unit-tanks (D/T No.29 ∿ No.54), it increases. After bewilderment during four gaps, it reaches 30°, stays on the value for fifteen gaps and then gradually decreases to 16° at D/T No.87. Mean phase at each gap corresponding to the injection energy of 750 keV (± 0.1 %) is also drawn in Fig.6. Except for several gaps around D/T No.13, mean phase oscillates around the synchronous phase. The above-mentioned behavior makes it difficult to follow the complete synchronous phase law experiment. The phase oscillation, rms phase spread and rms energy spread at this condition are shown in Figs.7, 8(a) and 8(b) respectively.

The axial mean field $\bar{E}$ changed from the initial value $\bar{E}_0$ is expressed by

$$\bar{E} = \bar{E}_0\beta\{1 + \alpha(2z/L - 1)\} \tag{30}$$

where β and α are constants which are called here field level and slope respectively. Corresponding to some values of field level and slope, the synchronous phase changes as shown in Figs.9 and 10. The value at D/T 56 does not become real until the field level is enhanced to 1.145 and it is roughly constant for the variation of slope because it is situated nearly in the middle of the cavity. Figs.11, 12 and 13 shows the phase oscillation, energy spectrum and rms energy and phase spread respectively for the slope 0.0 and Figs. 14, 15 and 16 for the field level 1.0.

For $\alpha = 0.0$ it seems preferable to operate at $\beta = 1.05$ in respect of phase oscillation and energy spread but mean energy becomes 20.46 MeV, which is rather lower than the design value. For a constant field level $\beta = 1.0$, the phase oscillation behaves singularly against the slope. At positive values the phase and energy spread is large in the early gaps and moderate in the later gaps. At negative values, the fairly regular oscillation is suddenly disordered after about 56-th gap. Correspondingly the energy spectrum after whole acceleration is better at positive slopes than negatives ones. The bahavior can also be infered by Fig.10 to some extent. It can therefore be concluded that to operate at $\alpha = 0$ or at a little positive α is most adequate. However it shows that our purpose of synchronous or linear phase law experiment is not fully attained. Fig.17 shows the calculated mean energy, rms energy spread and capture efficiency versus tank field level. At $\beta = 1.0$ and $\alpha = +0.1$, rms energy spread shows the sharp minimum but capture efficiency becomes relatively low.

5. Experimental Results

By a pair of bending magnets located after the second π-section, the accelerated beam is led to the analyser magnet (Fig.18). The detector has 48 channels and the energy resolution ($\Delta E/E$) of 0.1 %. The debuncher is situated between two π-sectional quadrupole magnets. Therefore on the one hand the effect of the debuncher can be measured by the analyser, on the other hand it cannot completely be avoided even if it is detuned from the resonant frequency. The field in the tank attained by moving four end tuner is shown in Fig.5. As described in Chap.3, it is measured by ten monitor probes under the assumption that at field level = 1.0 and slope = 0.0 the regulated field by the bead perturbation method in Figs.2, 3 and 4 is given.

The measured energy spectrum at slope 0.0 is shown in Fig.19. It was measured at the current of 20 mA, so that the space charge effect does not become noticeable and the signal to noise ratio did to become too worse. The buncher was not operated at this experiment. As it is not a cavity type, there would be no increase of energy spread against the injected beam 750 keV ± 0.1 %. Experimental rms energy spread, mean energy and normalized transmitted current I_0/I_i as the function of field level are shown in Fig.20 as well as the computational results. Experimental field level is written in an arbitrary scale, but field level 1.0 in the figure is the condition around which the linac is usually operated. According to the experiments the mean energy E_m shows the variation of the curve of third order around the field level 0.993 at which E_m is 20.65 MeV. In the narrower region the mean energy changes in proportion to the field level. However the calculated results show a nearly constant energy 20.65 MeV around $\beta = 0.997$. Fig.21 shows the same experiments for several slope values with higher current around 100 mA. Field level of the experimental and calculated value is relatively fitted by the mean energy at slope 0.0.

6. Conclusion

The phase oscillations are calculated using the data obtained by bead perturbation. According to the field measurement, a constant synchronous phase is not maintained throughout the whole gaps. However by changing the field level and slope, we could follow the linear synchronous phase law to some extent. Irrespective of the abrupt change of synchronous phase around D/T No.56, the particles do not escape from the acceleration if the field level and slope is not largely changed. In the present experiment, we did not find out any reason to operate at any other operational condition. Further it must be mentioned that after the field measurement by the bead perturbation method and before this experiment, the first sixteen drift tubes were replaced because of deterioration of electric insulation. Therefore it is uncertain that the initial field is completely reproduced. We are planning to measure the field by the same method in the near future.

Acknowledgment

We would like to express our sincere thanks to Prof. H. Baba and Messers. S. Anami, T. Kakuyama, T. Takenaka and Y. Terayama. The experiments were carried out by all the members of linac group.

References

1) K. Batchelor, R. Chasman and N. Fewell, "Calculation and Measurements on Reduction of the Energy Spread and the Variation in Mean Energy of the 200 MeV Linac Beam at Brookhaven", Proc. 1972 Linear Accelerator Conf., Los Alamos, LA-5115, 41 (1972).

2) G.W. Wheeler, "Performance of the BNL 200 MeV Proton Linear Accelerator", Proc. U.S.-Japan Seminar on High Energy Accelerator Science, Tokyo and Tsukuba, 269 (1973).

3) S. Okumura, "On Methods for Calculating the Field Distribution in a Proton Linac Cavity", Proc. 1976 Linear Accelerator Conf., Chalk River, p.394 (1976).

4) Working Group for Construction of Proton Synchrotron, "Progress Report of Injector Working Group 1", SJC-A-67-2 (1967).

5) M. Martini and D.J. Warner, "Numerical Calculations of Linear Accelerator Cavities", CERN 68-11 (1968).

6) S. Okumura and D.A. Swenson, "Bead Perturbation Measurement for the KEK Linac Cavity", KEK-74-15 (1975).

7) E.L. Hubbard, "Linear Ion Accelerators", Advances in Electronics and Electron Physics 25, 65 (1968).

8) L. Smith, "Linear Accelerators", Handbuch der Physik, XLIV, 346 (1959).

9) R.L. Gluckstern, "Space Charge Effects", Linear Accelerator, p.827 (North Holland Publ. Co., 1969).
S. Okumura, T. Nishikawa and H. Yoshikawa, "Experimental Study on the Space-Charge Effect in Proton Linacs by an Electron Model", Particle Accelerator 2, 279 (1971).

Table 1

CELL N	CELL LENGTH(cm)	GAP LENGTH(cm)	ENERGY IN (MeV)	ENERGY GAIN (MeV)	BETA IN	DRIFT TUBE.LENGTH(cm)	BORE (cm)	RHC (cm)	RH (cm)	SD (cm)
1	6.020	1.275	0.7500	0.0507	0.03996	2.3290	2.0	1.0	2.0	179.28
2	6.237	1.331	0.8007	0.0538	0.04128	4.8314	2.0	1.0	2.0	179.28
3	6.441	1.385	0.8545	0.0568	0.04264	4.9793	2.0	1.0	2.0	179.28
4	6.651	1.440	0.9113	0.0598	0.04404	5.1328	2.0	1.0	2.0	179.58
5	6.864	1.497	0.9712	0.0630	0.04546	5.2885	2.0	1.0	2.0	179.58
6	7.083	1.556	1.0341	0.0662	0.04690	5.4461	2.0	1.0	2.0	179.58
7	7.305	1.616	1.1003	0.0694	0.04838	5.6076	2.0	1.0	2.0	179.58
8	7.531	1.678	1.1698	0.0728	0.04988	5.7700	2.0	1.0	2.0	179.90
9	7.760	1.741	1.2425	0.0762	0.05141	5.9358	2.0	1.0	2.0	180.90
10	7.992	1.806	1.3187	0.0796	0.05296	6.1020	2.0	1.0	2.0	180.90
11	8.229	1.872	1.3983	0.0831	0.05453	6.2717	2.0	1.0	2.0	180.90
12	8.467	1.940	1.4814	0.0866	0.05612	6.4420	2.0	1.0	2.0	180.90
13	8.709	2.009	1.5680	0.0902	0.05773	6.6137	2.0	1.0	2.0	180.90
14	8.955	2.079	1.6581	0.0938	0.05937	6.7877	2.0	1.0	2.0	180.90
15	9.202	2.151	1.7519	0.0974	0.06102	6.9625	2.0	1.0	2.0	180.90
16	9.451	2.225	1.8492	0.1010	0.06269	7.1380	2.0	1.0	2.0	179.90
17	9.704	2.300	1.9503	0.1047	0.06437	7.3151	2.0	1.0	2.0	180.26
18	9.958	2.376	2.0549	0.1084	0.06607	7.4931	2.0	1.0	2.0	180.26
19	10.215	2.453	2.1633	0.1121	0.06779	7.6718	2.0	1.0	2.0	180.26
20	10.474	2.532	2.2754	0.1158	0.06951	7.8511	2.0	1.0	2.0	180.26
21	10.734	2.613	2.3912	0.1196	0.07126	8.0314	2.0	1.0	2.0	180.26
22	10.996	2.694	2.5108	0.1233	0.07301	8.2114	2.0	1.0	2.0	180.26
23	11.260	2.777	2.6341	0.1271	0.07477	8.3927	2.0	1.0	2.0	180.26
24	11.525	2.861	2.7612	0.1309	0.07655	8.5735	2.0	1.0	2.0	180.26
25	11.792	2.946	2.8921	0.1347	0.07833	8.7549	2.0	1.0	2.0	180.26
26	12.060	3.032	3.0268	0.1385	0.08013	8.9366	2.0	1.0	2.0	180.26
27	12.330	3.120	3.1653	0.1424	0.08193	9.1182	2.0	1.0	2.0	180.26
28	12.600	3.201	3.3077	0.1462	0.08375	9.3003	2.0	1.0	2.0	180.26
29	12.869	3.284	3.4539	0.1457	0.08556	9.4817	2.5	1.26	2.0	181.43
30	13.130	3.372	3.5996	0.1448	0.08734	9.6573	2.5	1.26	2.0	181.43
31	13.387	3.459	3.7444	0.1482	0.08907	9.8272	2.5	1.26	2.0	181.43
32	13.646	3.548	3.8926	0.1516	0.09081	9.9986	2.5	1.26	2.0	181.43
33	13.906	3.624	4.0442	0.1550	0.09255	10.1693	2.5	1.26	2.0	181.43
34	14.166	3.703	4.1992	0.1583	0.09429	10.3394	2.5	1.70	2.0	181.03
35	14.427	3.794	4.3575	0.1617	0.09604	10.5094	2.5	1.70	2.0	181.03
36	14.688	3.885	4.5192	0.1650	0.09779	10.6794	2.5	1.70	2.0	181.03
37	14.950	3.978	4.6842	0.1682	0.09955	10.8484	2.5	1.70	2.0	181.03
38	15.212	4.072	4.8524	0.1714	0.10131	11.0171	2.5	1.70	2.0	181.03
39	15.475	4.167	5.0238	0.1746	0.10307	11.1855	2.5	1.70	2.0	181.03
40	15.737	4.262	5.1984	0.1777	0.10483	11.3530	2.5	1.70	2.0	181.03
41	15.999	4.358	5.3761	0.1807	0.10659	11.5194	2.5	1.70	2.0	181.03
42	16.262	4.455	5.5568	0.1837	0.10835	11.6856	2.5	1.70	2.0	181.03
43	16.524	4.535	5.7405	0.1866	0.11011	11.8505	2.5	1.70	2.0	181.03
44	16.786	4.617	5.9272	0.1895	0.11187	12.0148	2.5	2.20	2.0	181.43
45	17.047	4.716	6.1167	0.1923	0.11363	12.1780	2.5	2.20	2.0	181.43
46	17.308	4.816	6.3089	0.1950	0.11538	12.3401	2.5	2.20	2.0	181.43
47	17.569	4.916	6.5039	0.1976	0.11713	12.5013	2.5	2.20	2.0	181.43
48	17.829	5.016	6.7015	0.2001	0.11888	12.6611	2.5	2.20	2.0	181.43
49	18.088	5.117	6.9015	0.2025	0.12062	12.8201	2.5	2.20	2.0	181.43
50	18.346	5.219	7.1041	0.2048	0.12236	12.9774	2.5	2.20	2.0	181.43
51	18.604	5.320	7.3089	0.2071	0.12409	13.1338	2.5	2.20	2.0	181.43
52	18.860	5.423	7.5160	0.2092	0.12582	13.2886	2.5	2.20	2.0	181.43
53	19.115	5.525	7.7251	0.2112	0.12754	13.4419	2.5	2.20	2.0	181.43
54	19.372	5.629	7.9363	0.2131	0.12925	13.5938	2.5	2.20	2.0	181.43
55	19.604	5.724	8.1494	0.2148	0.13095	13.7476	2.5	2.20	2.0	181.43
56	20.008	5.501	8.3642	0.2168	0.13264	13.8691	2.5	2.20	2.0	181.43
57	20.139	5.167	8.5811	0.2471	0.13432	14.2227	2.5	0.5	4.0	181.43
58	20.305	5.232	8.8282	0.2797	0.13622	14.8711	2.5	0.5	4.0	181.43
59	20.773	5.416	9.1079	0.2874	0.13833	15.2740	2.5	0.5	4.0	181.43
60	21.073	5.535	9.3954	0.2929	0.14046	15.4407	2.5	0.5	4.0	181.43
61	21.394	5.663	9.6882	0.2986	0.14260	15.6353	2.5	0.5	4.0	181.43
62	21.714	5.793	9.9868	0.3043	0.14475	15.8258	2.5	0.5	4.0	181.43
63	22.035	5.924	10.2911	0.3101	0.14690	16.0159	2.5	0.5	4.0	181.43
64	22.357	6.058	10.6012	0.3159	0.14906	16.2056	2.5	0.5	4.0	181.43
65	22.680	6.192	10.9171	0.3217	0.15123	16.3941	2.5	0.5	4.0	181.43
66	23.005	6.329	11.2388	0.3276	0.15340	16.5821	2.5	0.5	4.0	181.43
67	23.330	6.467	11.5665	0.3335	0.15558	16.7693	2.5	0.5	4.0	181.43
68	23.656	6.607	11.9000	0.3395	0.15777	16.9559	2.5	0.5	4.0	181.43
69	23.982	6.749	12.2394	0.3454	0.15996	17.1414	2.5	0.5	4.0	181.43
70	24.310	6.892	12.5849	0.3515	0.16216	17.3259	2.5	0.5	4.0	181.43
71	24.639	7.037	12.9363	0.3575	0.16436	17.5099	2.5	0.5	4.0	181.43
72	24.968	7.184	13.2938	0.3636	0.16657	17.6931	2.5	0.5	4.0	181.43
73	25.298	7.333	13.6574	0.3697	0.16878	17.8752	2.5	0.5	4.0	181.43
74	25.629	7.483	14.0272	0.3759	0.17100	18.0564	2.5	0.5	4.0	181.43
75	25.961	7.635	14.4031	0.3821	0.17323	18.2368	2.5	0.5	4.0	181.43
76	26.294	7.788	14.7852	0.3884	0.17546	18.4163	2.5	0.5	4.0	181.43
77	26.627	7.943	15.1737	0.3947	0.17770	18.5947	2.5	0.5	4.0	181.43
78	26.961	8.100	15.5884	0.4011	0.17994	18.7723	2.5	0.5	4.0	181.43
79	27.296	8.259	15.9695	0.4076	0.18218	18.9491	2.5	0.5	4.0	181.43
80	27.632	8.419	16.3771	0.4141	0.18443	19.1247	2.5	0.5	4.0	181.43
81	27.968	8.582	16.7912	0.4207	0.18669	19.2995	2.5	0.5	4.0	181.43
82	28.305	8.746	17.2119	0.4274	0.18895	19.4733	2.5	0.5	4.0	181.43
83	28.643	8.911	17.6392	0.4341	0.19122	19.6460	2.5	0.5	4.0	181.43
84	28.982	9.079	18.0733	0.4410	0.19349	19.8181	2.5	0.5	4.0	181.43
85	29.322	9.248	18.5143	0.4479	0.19577	19.9890	2.5	0.5	4.0	181.43
86	29.663	9.419	18.9622	0.4550	0.19806	20.1589	2.5	0.5	4.0	181.43
87	30.006	9.593	19.4171	0.4622	0.20035	20.3277	2.5	0.5	4.0	181.43
88	30.337	9.762	19.8793	0.4693	0.20264	20.4980	2.5	0.5	4.0	181.43
89	30.694	9.971	20.3486	0.4776	0.20495	20.6519	2.5	0.5	4.0	181.43
90	0.0	0.0	20.8262	0.0	0.20726	10.4459	2.5	0.5	4.0	181.43

Table 2

CELL N	SUM LENGTH (cm)	AVERAGE FIELD (MV/cm)	TRAN.T. FACTOR	DERIV. T.T.F	SHUNT IMPED.(Mohm/m)	EFF.SHUNT IMPED.(Mohm/m)	NO.BEAM SUM POWER (MW)	100MA SUM POWER
1	6.020	0.0150	0.6235	0.0984	65.28	25.37	0.0021	0.0071
2	12.256	0.0150	0.6377	0.0966	65.75	26.74	0.0042	0.0147
3	18.697	0.0151	0.6504	0.0947	66.17	27.99	0.0064	0.0226
4	25.348	0.0151	0.6626	0.0928	66.59	29.24	0.0087	0.0308
5	32.212	0.0151	0.6744	0.0909	67.01	30.47	0.0110	0.0395
6	39.295	0.0151	0.6856	0.0891	67.41	31.68	0.0135	0.0485
7	46.600	0.0152	0.6962	0.0872	67.80	32.87	0.0159	0.0579
8	54.130	0.0152	0.7064	0.0855	68.18	34.02	0.0185	0.0677
9	61.890	0.0152	0.7159	0.0837	68.55	35.13	0.0211	0.0780
10	69.883	0.0153	0.7249	0.0820	68.90	36.21	0.0238	0.0886
11	78.111	0.0153	0.7334	0.0803	69.23	37.24	0.0266	0.0997
12	86.579	0.0153	0.7413	0.0786	69.55	38.21	0.0295	0.1113
13	95.288	0.0154	0.7486	0.0771	69.85	39.14	0.0324	0.1232
14	104.243	0.0154	0.7554	0.0755	70.13	40.02	0.0354	0.1356
15	113.445	0.0154	0.7617	0.0740	70.39	40.84	0.0385	0.1485
16	122.896	0.0155	0.7675	0.0726	70.63	41.60	0.0417	0.1618
17	132.600	0.0155	0.7728	0.0713	70.85	42.31	0.0450	0.1755
18	142.558	0.0156	0.7776	0.0700	71.05	42.96	0.0484	0.1898
19	152.773	0.0156	0.7820	0.0687	71.22	43.56	0.0519	0.2045
20	163.247	0.0156	0.7860	0.0676	71.37	44.05	0.0555	0.2196
21	173.981	0.0157	0.7896	0.0665	71.50	44.57	0.0592	0.2353
22	184.977	0.0157	0.7928	0.0655	71.60	45.00	0.0630	0.2514
23	196.236	0.0158	0.7956	0.0645	71.68	45.37	0.0669	0.2680
24	207.761	0.0158	0.7982	0.0637	71.73	45.70	0.0709	0.2851
25	219.553	0.0159	0.8005	0.0629	71.75	45.97	0.0750	0.3027
26	231.613	0.0159	0.8025	0.0622	71.74	46.20	0.0793	0.3208
27	243.943	0.0160	0.8042	0.0616	71.71	46.38	0.0837	0.3394
28	256.543	0.0160	0.8058	0.0611	71.66	46.53	0.0882	0.3586
29	269.411	0.0161	0.7837	0.0613	72.02	44.23	0.0928	0.3777
30	282.541	0.0161	0.7609	0.0614	72.59	42.03	0.0975	0.3969
31	295.928	0.0162	0.7613	0.0608	72.71	42.14	0.1023	0.4165
32	309.574	0.0162	0.7614	0.0603	72.81	42.21	0.1072	0.4366
33	323.480	0.0163	0.7613	0.0598	72.92	42.26	0.1122	0.4572
34	337.646	0.0163	0.7608	0.0593	73.01	42.26	0.1174	0.4782
35	352.073	0.0164	0.7601	0.0589	73.11	42.24	0.1227	0.4996
36	366.761	0.0164	0.7591	0.0584	73.20	42.17	0.1281	0.5216
37	381.711	0.0165	0.7577	0.0580	73.28	42.08	0.1337	0.5439
38	396.923	0.0166	0.7561	0.0577	73.36	41.94	0.1394	0.5668
39	412.397	0.0166	0.7542	0.0573	73.44	41.77	0.1452	0.5900
40	428.134	0.0167	0.7520	0.0570	73.51	41.57	0.1512	0.6138
41	444.134	0.0167	0.7495	0.0567	73.58	41.33	0.1573	0.6379
42	460.395	0.0168	0.7467	0.0567	73.64	41.06	0.1635	0.6625
43	476.919	0.0169	0.7437	0.0567	73.69	40.76	0.1699	0.6876
44	493.705	0.0169	0.7403	0.0566	73.75	40.42	0.1764	0.7131
45	510.752	0.0170	0.7367	0.0566	73.79	40.05	0.1831	0.7390
46	528.060	0.0171	0.7328	0.0566	73.84	39.65	0.1899	0.7653
47	545.629	0.0171	0.7286	0.0566	73.87	39.22	0.1969	0.7921
48	563.457	0.0172	0.7241	0.0565	73.91	38.75	0.2041	0.8192
49	581.545	0.0173	0.7194	0.0565	73.93	38.26	0.2114	0.8468
50	599.891	0.0174	0.7144	0.0565	73.96	37.75	0.2189	0.8748
51	618.495	0.0174	0.7091	0.0565	73.98	37.20	0.2265	0.9031
52	637.355	0.0175	0.7036	0.0564	73.99	36.63	0.2343	0.9319
53	656.470	0.0176	0.6979	0.0564	74.00	36.04	0.2423	0.9610
54	675.842	0.0177	0.6918	0.0564	74.01	35.42	0.2505	0.9905
55	695.446	0.0177	0.6861	0.0563	74.01	34.84	0.2589	1.0203
56	715.454	0.0178	0.6756	0.0563	74.00	33.78	0.2674	1.0505
57	735.593	0.0179	0.7616	0.0503	75.97	44.06	0.2759	1.0838
58	755.898	0.0180	0.8511	0.0446	77.90	56.43	0.2844	1.1202
59	776.671	0.0181	0.8509	0.0448	77.72	56.28	0.2931	1.1576
60	797.743	0.0182	0.8507	0.0451	77.60	56.16	0.3020	1.1959
61	819.137	0.0182	0.8504	0.0454	77.45	56.00	0.3112	1.2349
62	840.851	0.0183	0.8499	0.0457	77.29	55.83	0.3207	1.2748
63	862.886	0.0184	0.8493	0.0460	77.12	55.63	0.3303	1.3155
64	885.243	0.0185	0.8487	0.0463	76.94	55.41	0.3403	1.3570
65	907.923	0.0186	0.8479	0.0466	76.74	55.17	0.3505	1.3994
66	930.928	0.0187	0.8471	0.0469	76.52	54.91	0.3610	1.4426
67	954.258	0.0188	0.8461	0.0472	76.30	54.62	0.3718	1.4868
68	977.913	0.0189	0.8451	0.0475	76.06	54.32	0.3828	1.5318
69	1001.896	0.0190	0.8440	0.0477	75.81	54.00	0.3942	1.5777
70	1026.206	0.0191	0.8428	0.0480	75.54	53.66	0.4059	1.6245
71	1050.844	0.0192	0.8416	0.0483	75.26	53.30	0.4179	1.6723
72	1075.813	0.0193	0.8403	0.0486	74.96	52.93	0.4303	1.7210
73	1101.111	0.0194	0.8389	0.0489	74.65	52.54	0.4430	1.7707
74	1126.740	0.0195	0.8375	0.0492	74.33	52.14	0.4560	1.8213
75	1152.701	0.0196	0.8361	0.0495	73.99	51.72	0.4695	1.8730
76	1178.994	0.0197	0.8346	0.0498	73.64	51.30	0.4833	1.9256
77	1205.621	0.0198	0.8331	0.0501	73.27	50.86	0.4975	1.9793
78	1232.582	0.0199	0.8316	0.0504	72.89	50.41	0.5121	2.0340
79	1259.878	0.0200	0.8301	0.0507	72.50	49.95	0.5271	2.0898
80	1287.509	0.0201	0.8285	0.0510	72.08	49.48	0.5426	2.1467
81	1315.477	0.0202	0.8270	0.0513	71.66	49.01	0.5586	2.2047
82	1343.782	0.0203	0.8255	0.0516	71.22	48.53	0.5750	2.2639
83	1372.425	0.0204	0.8240	0.0519	70.76	48.05	0.5919	2.3242
84	1401.407	0.0206	0.8226	0.0522	70.29	47.56	0.6093	2.3857
85	1430.729	0.0207	0.8212	0.0525	69.80	47.07	0.6272	2.4484
86	1460.391	0.0208	0.8199	0.0529	69.30	46.59	0.6457	2.5124
87	1490.397	0.0209	0.8186	0.0532	68.78	46.09	0.6648	2.5777
88	1520.734	0.0210	0.8175	0.0535	68.27	45.62	0.6844	2.6443
89	1551.428	0.0211	0.8163	0.0538	67.69	45.10	0.7047	2.7123
90	1551.428	0.0211	0.0	0.0000	67.69	0.0	0.7047	2.7123

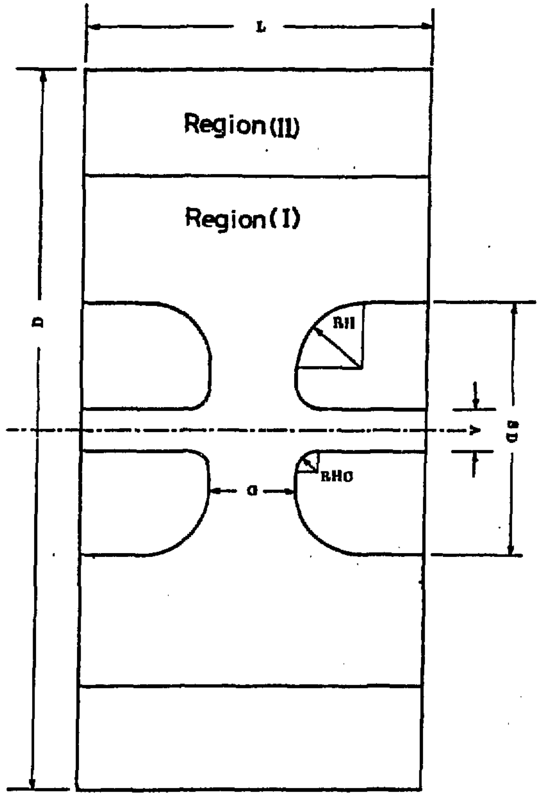

Fig.1 Unit-Cell

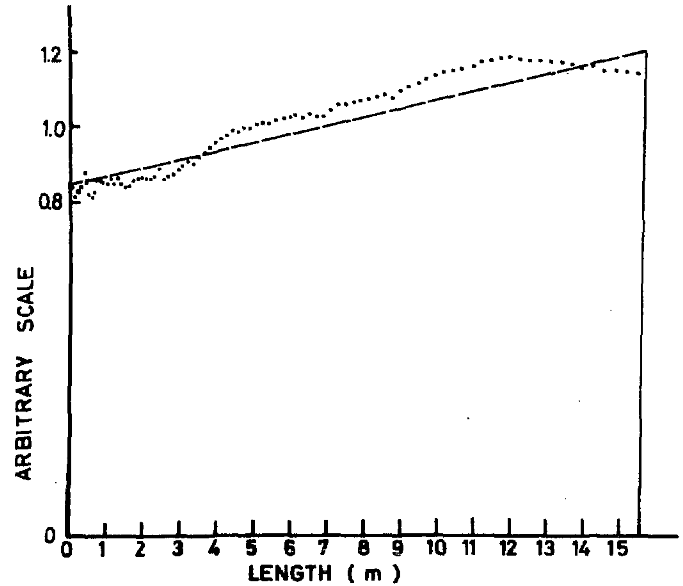

Fig.2 Average Axial Electric Field of TM_{010} Mode

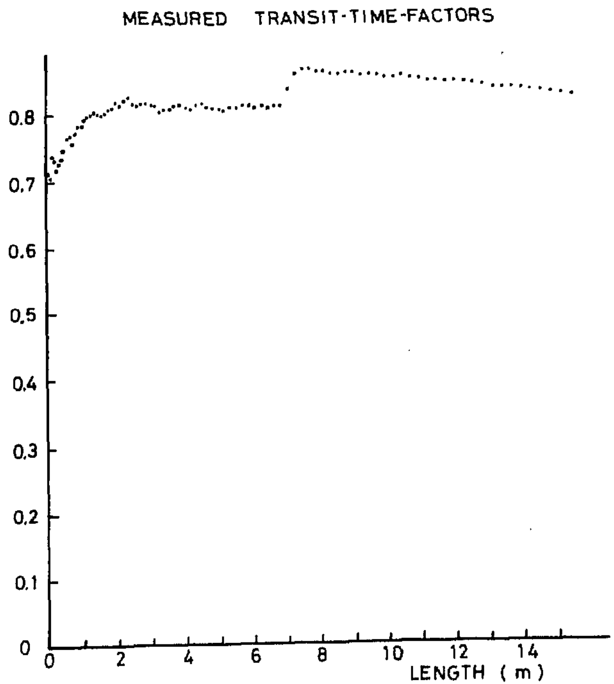

Fig.3 Measured Transit-Time Factors

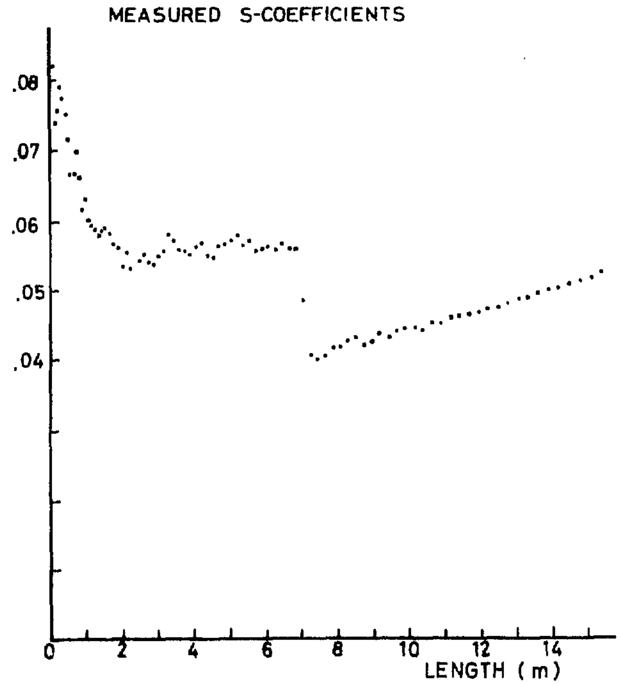

Fig.4 Measured S-Coefficients

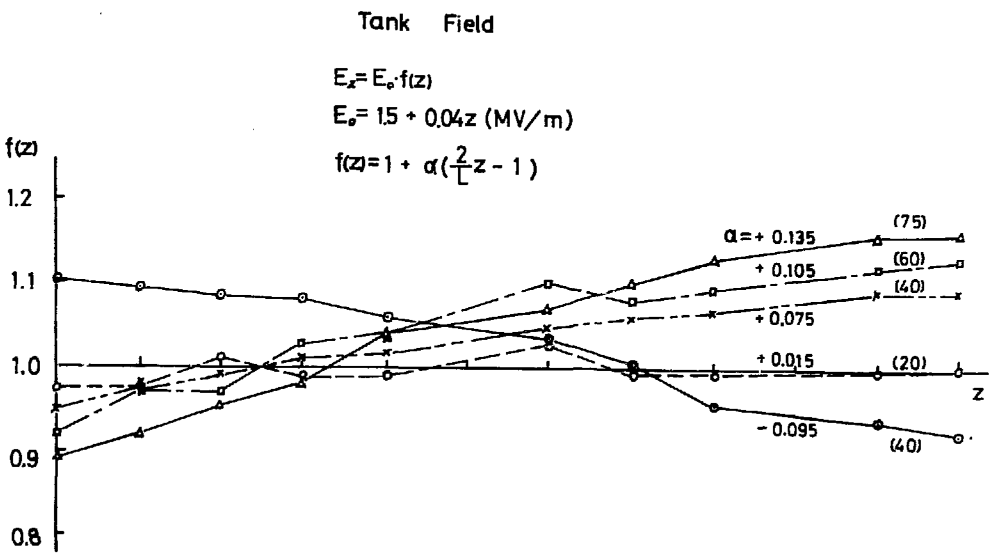

Fig.5 Measured Field Distribution for Various Tuner Positions

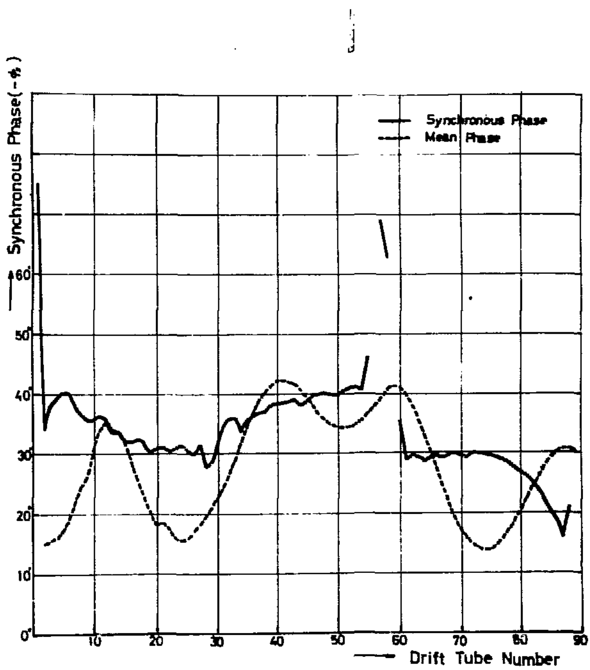

Fig.6 Synchronous Phase for Measured Average Electric Field and Transit-Time Factors and Mean Phase for Injection Energy of 750 keV (± 0.1 %).

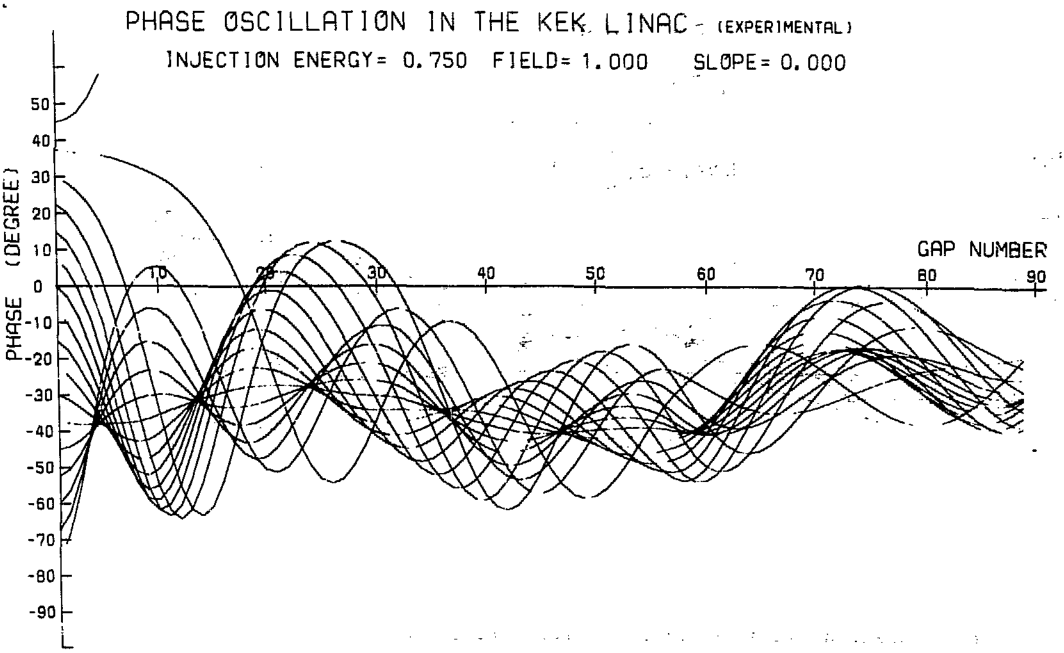

Fig.7 Phase Oscillation for Designed Value

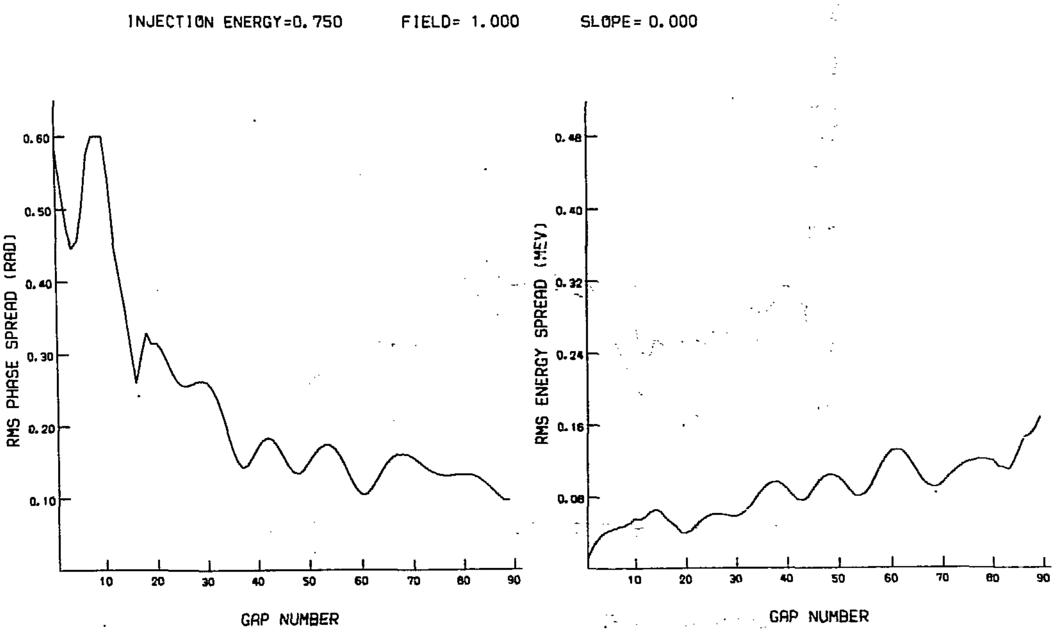

Fig.8 Rms Phase and Energy Spread for Designed Value

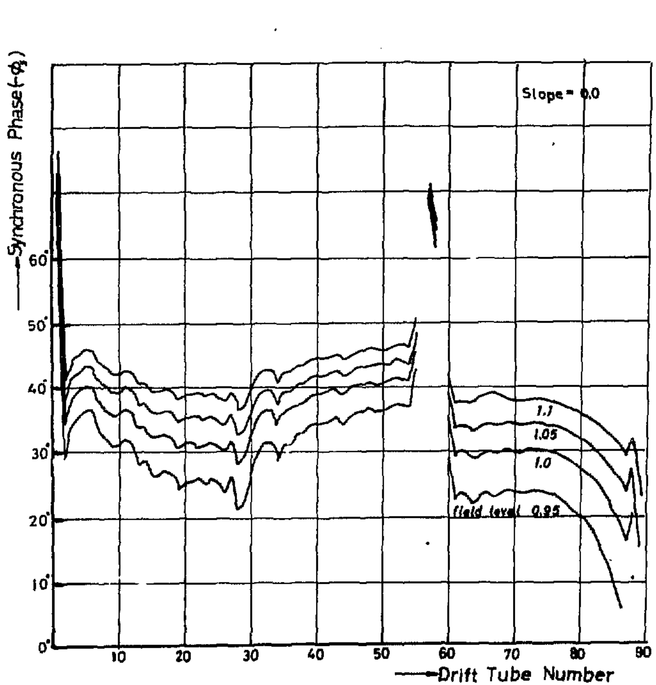

Fig.9 Synchronous Phase for Various Field Level at Slope 0.0

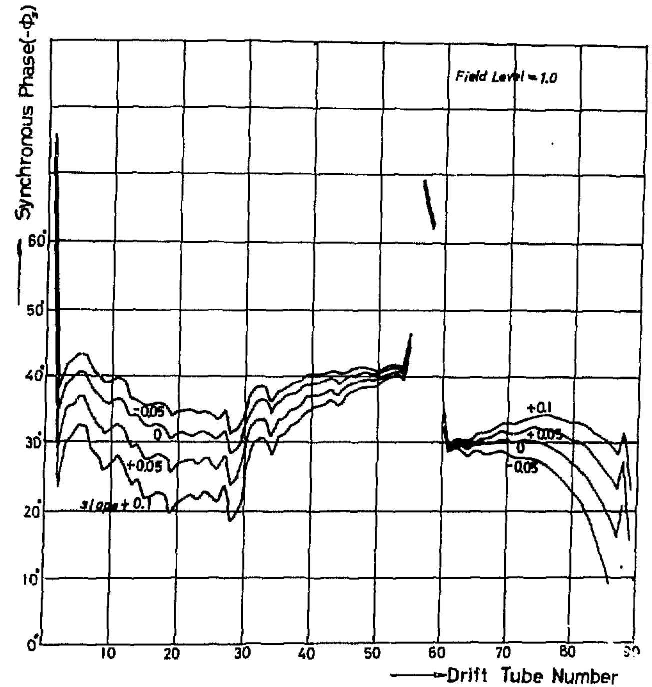

Fig.10 Synchronous Phase for Various Slope at Field Level 1.0

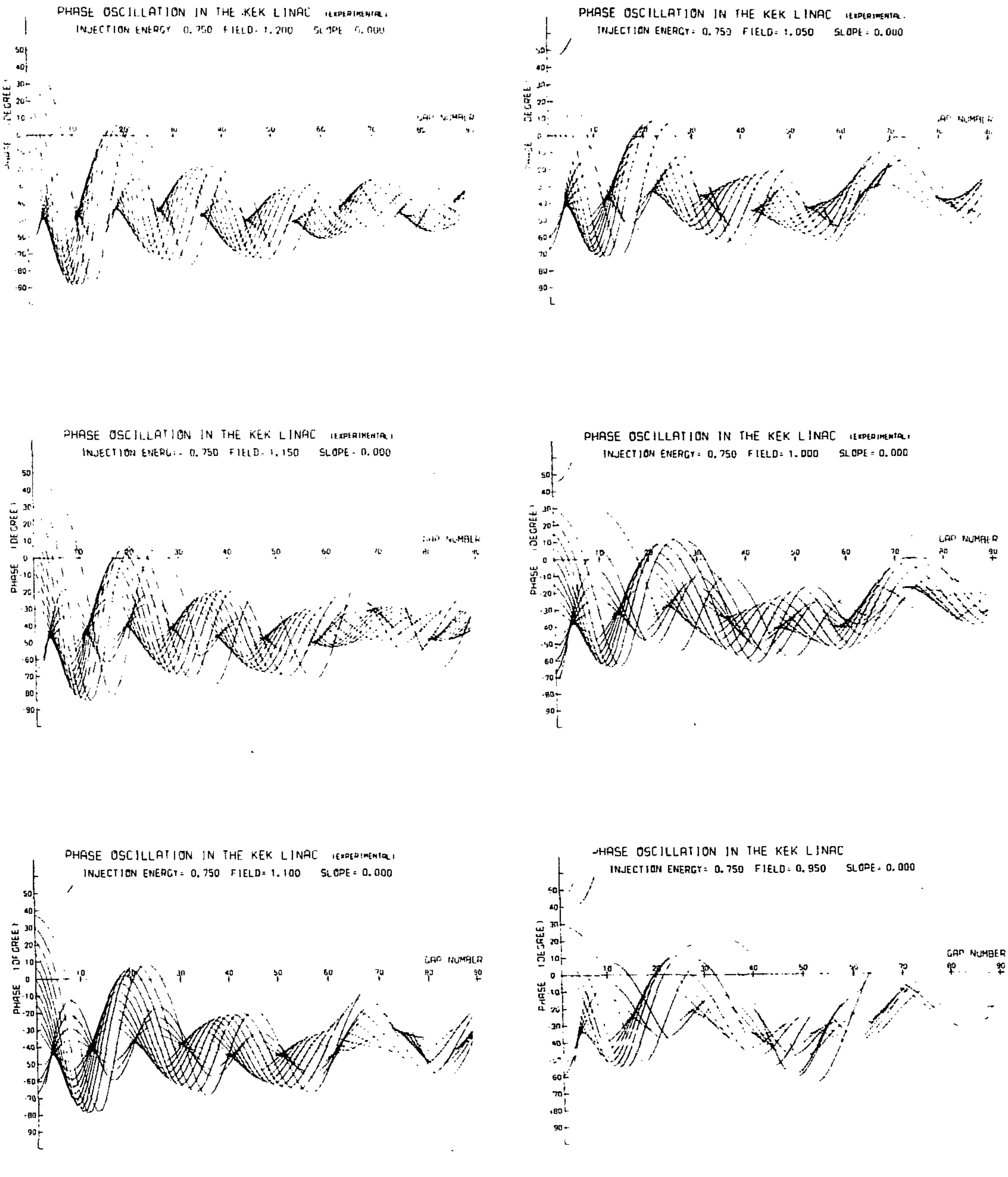

Fig.11 Phase Oscillation at Slope 0.0

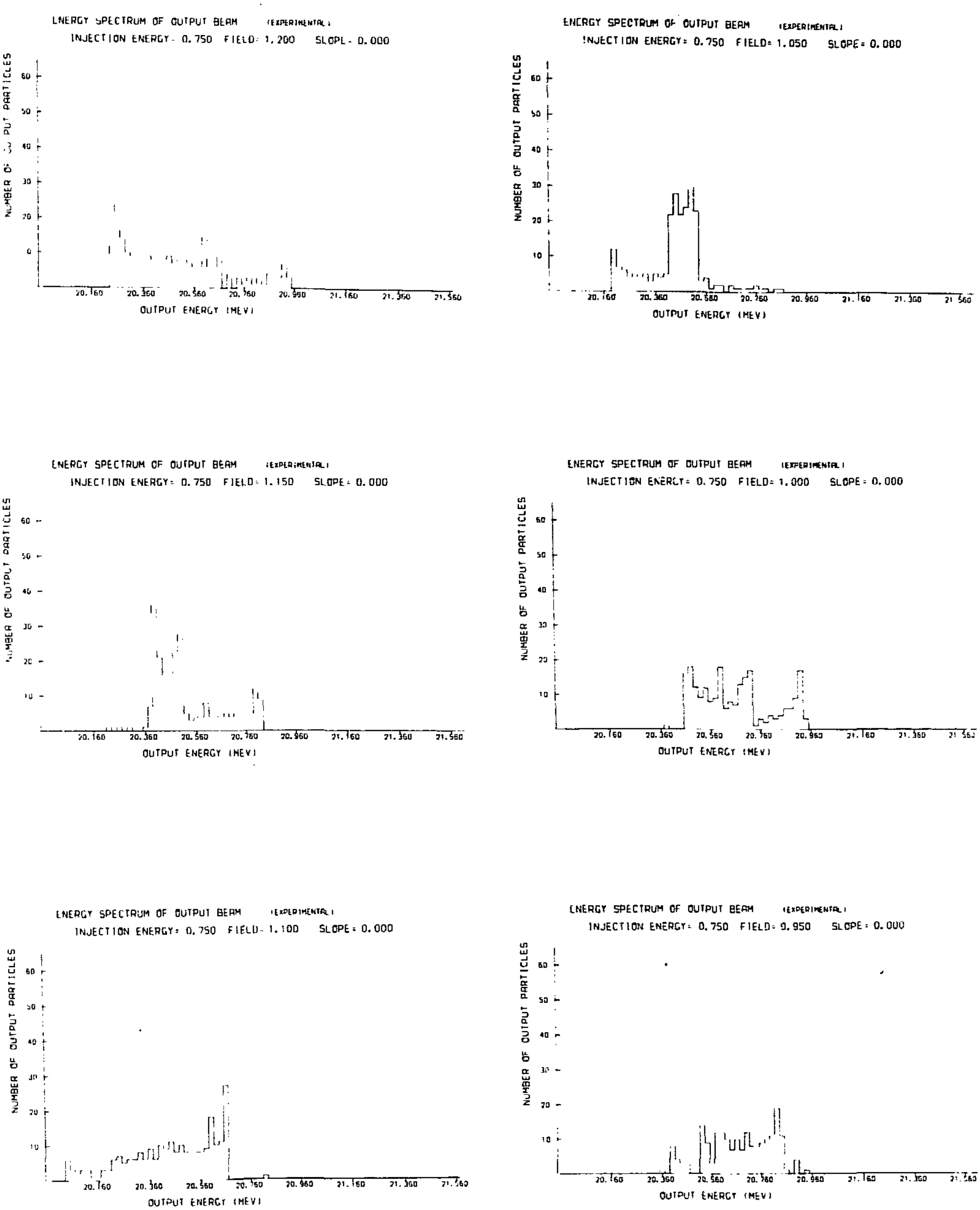

Fig.12 Energy Spectrum at Slope 0.0

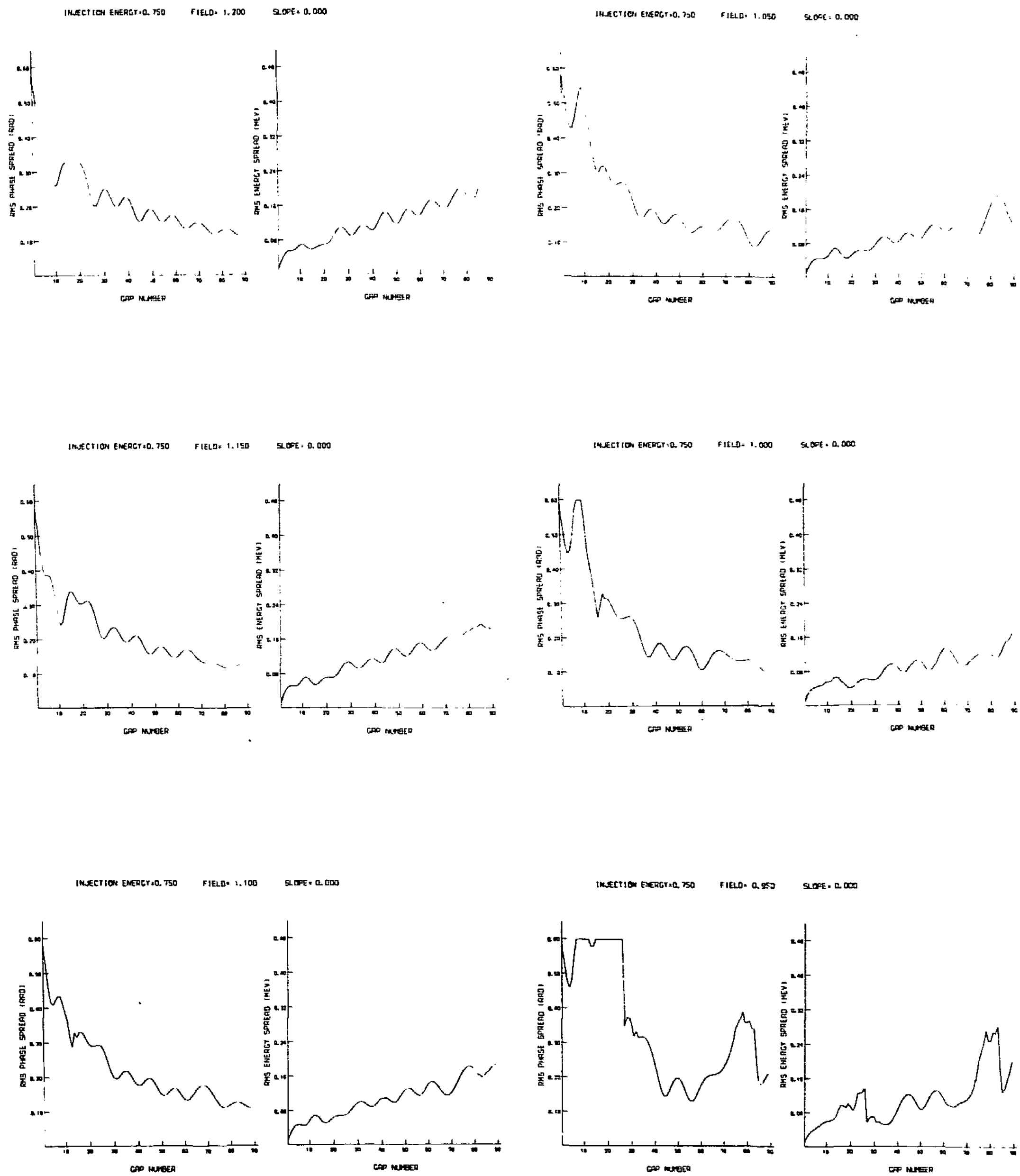

Fig.13 Rms Energy and Phase Spread at Slope 0.0

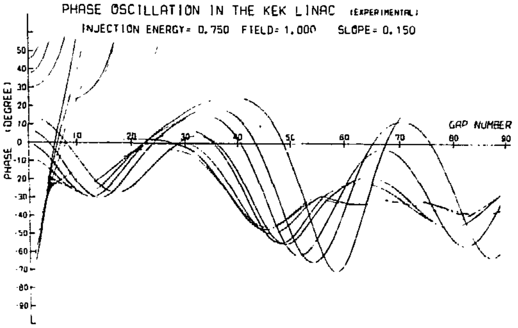

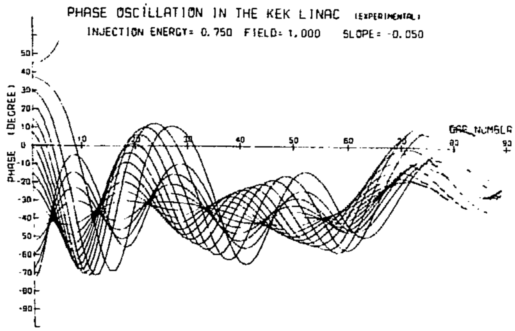

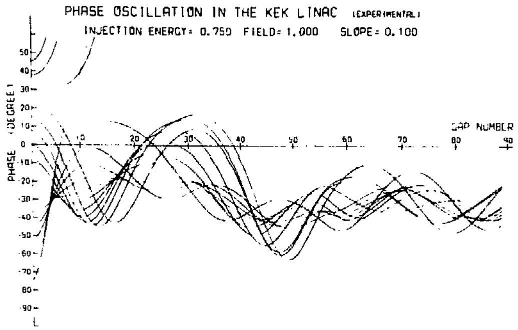

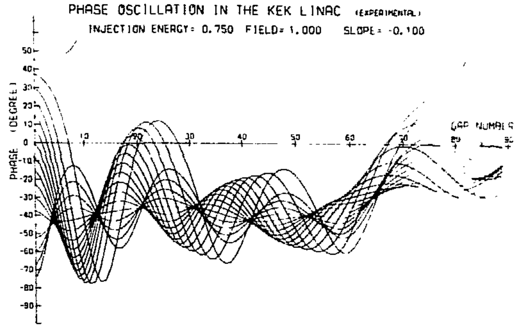

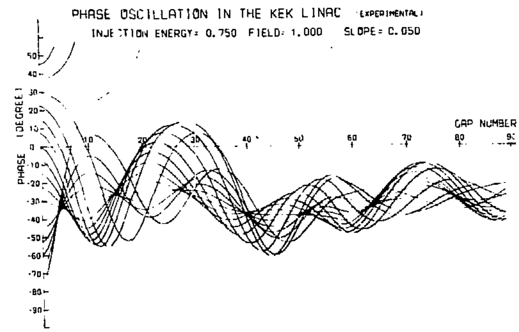

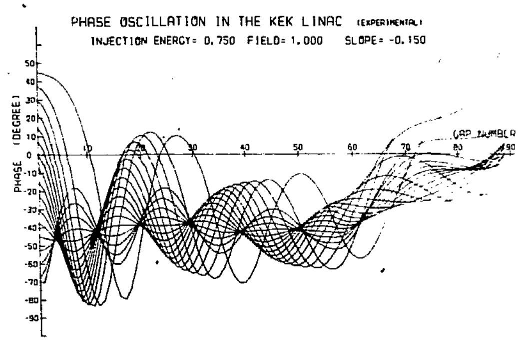

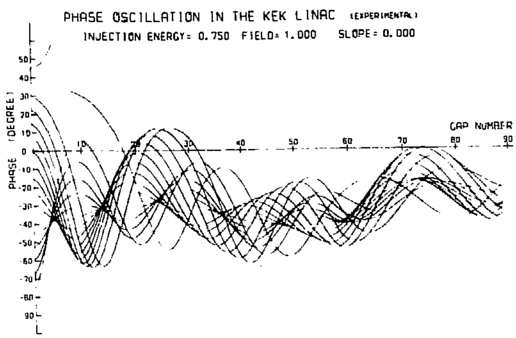

Fig.14 Phase Oscillation at Field Level 1.0

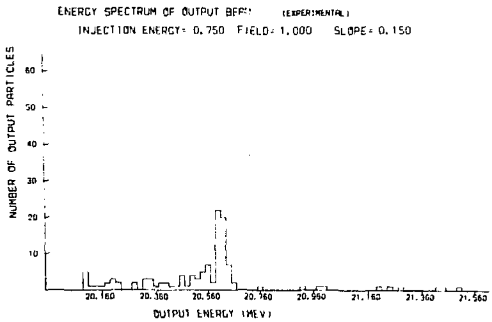

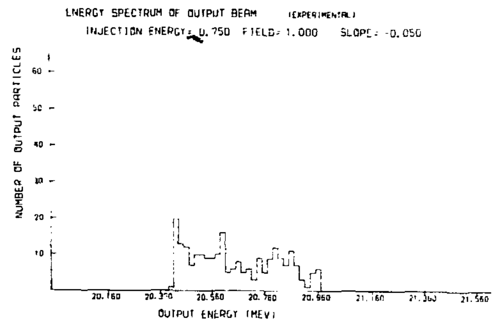

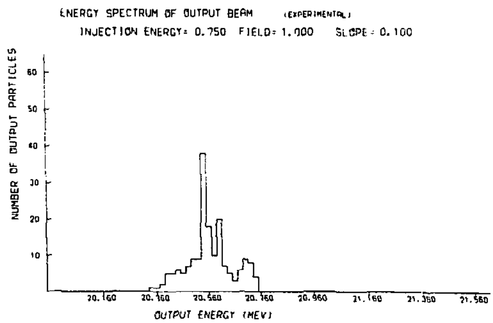

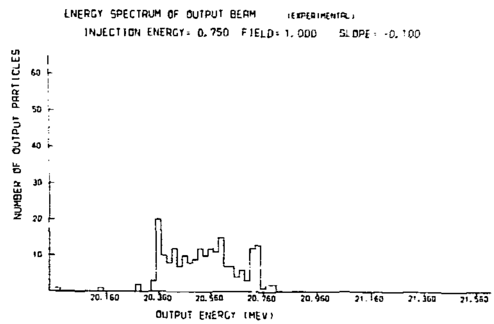

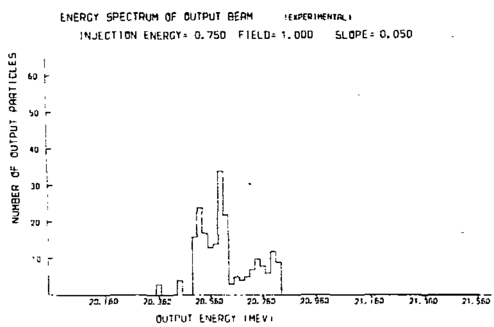

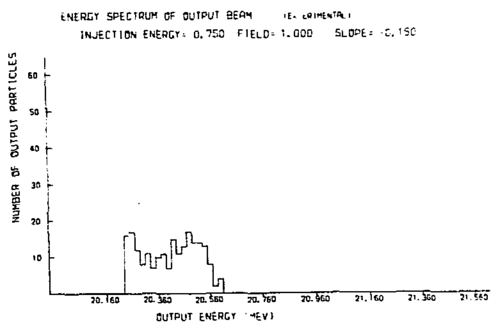

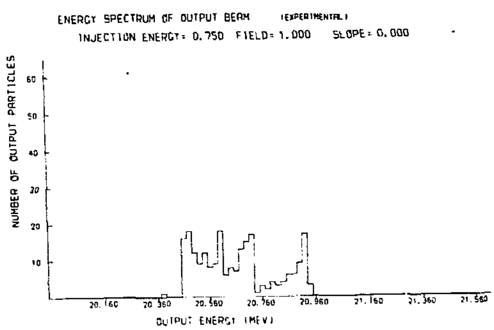

Fig.15 Energy Spectrum at Field Level 1.0

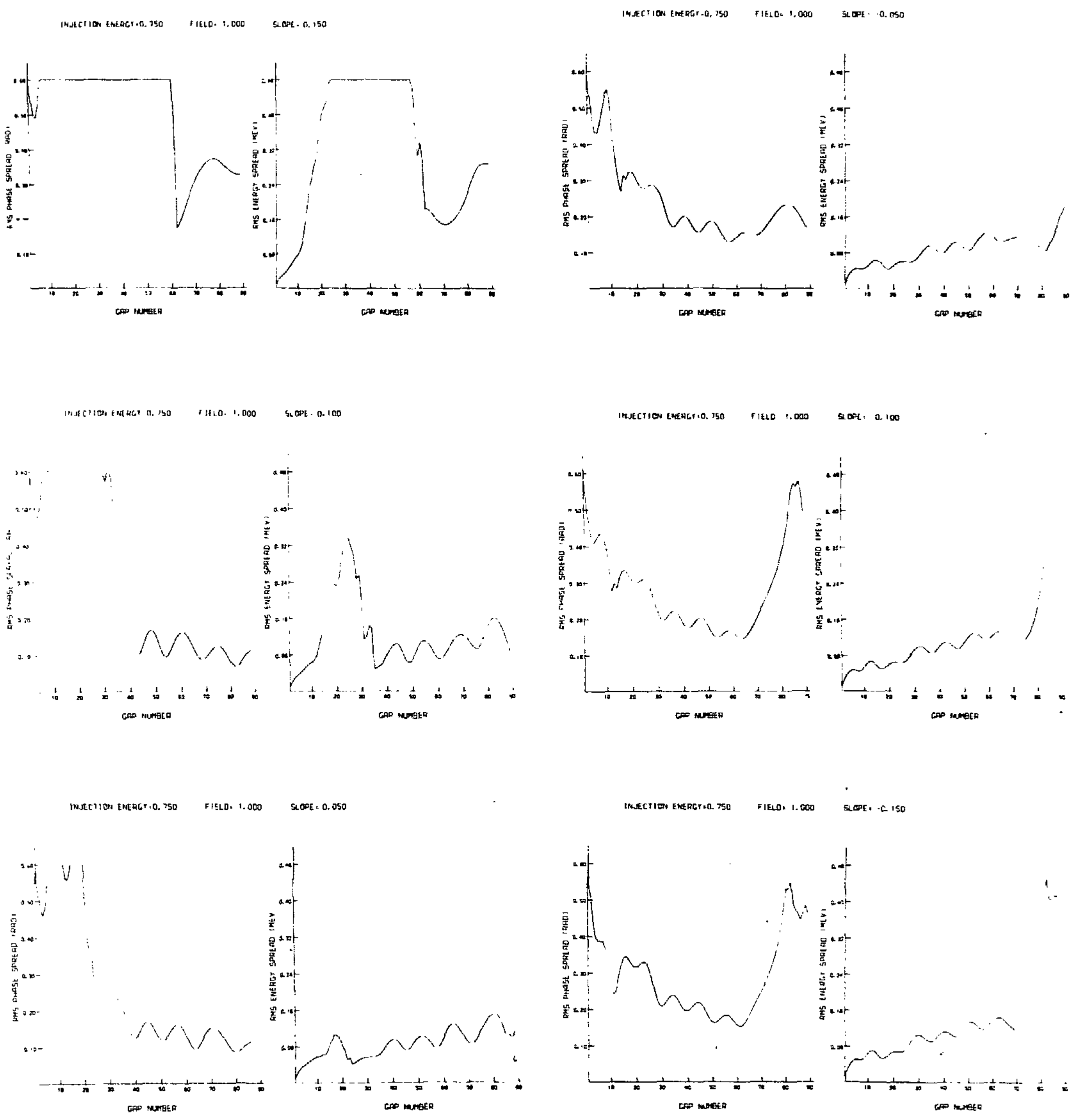

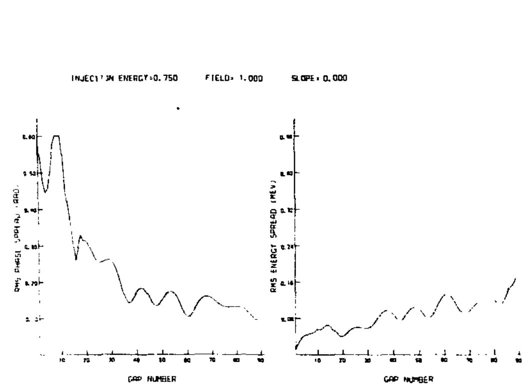

Fig.16 Rms Energy and Phase Spread at Field Level 1.0

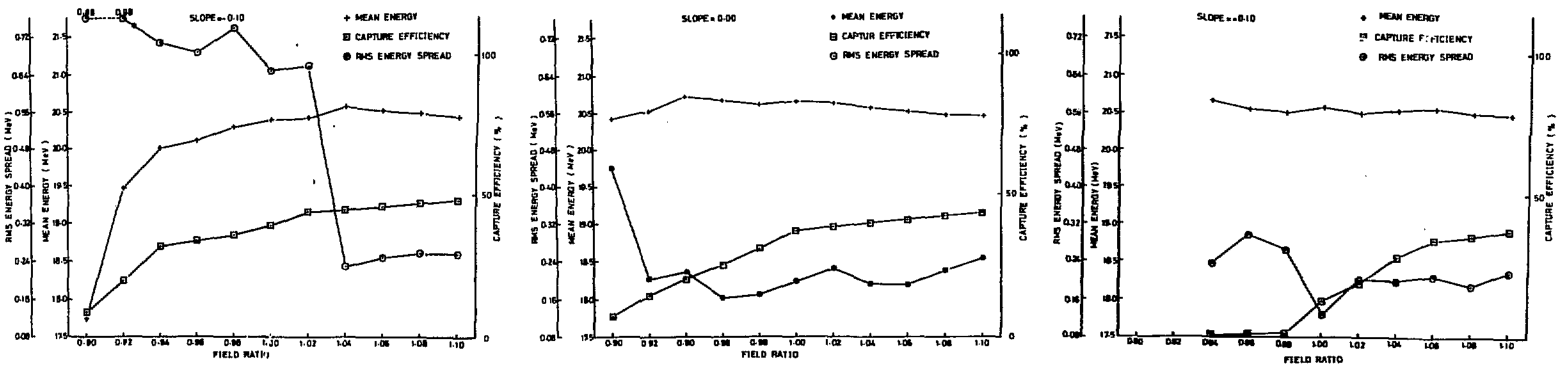

Fig.17 Calculated Mean Energy, Rms Energy Spread and Capture Efficiency versus Tank Field Level

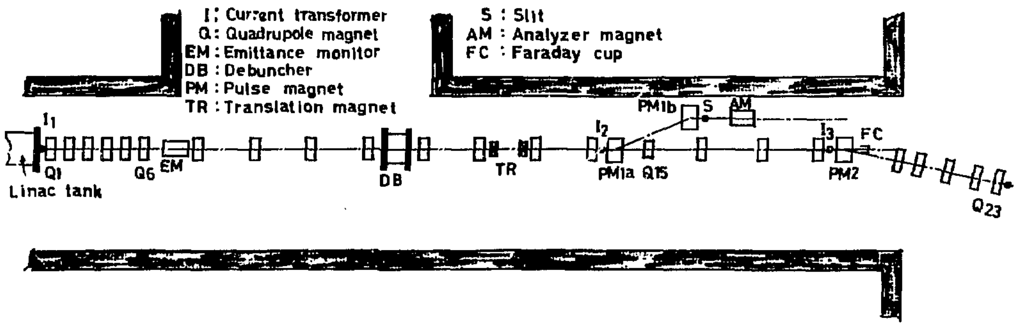

Fig.18 Linac to Booster Beam Transport System

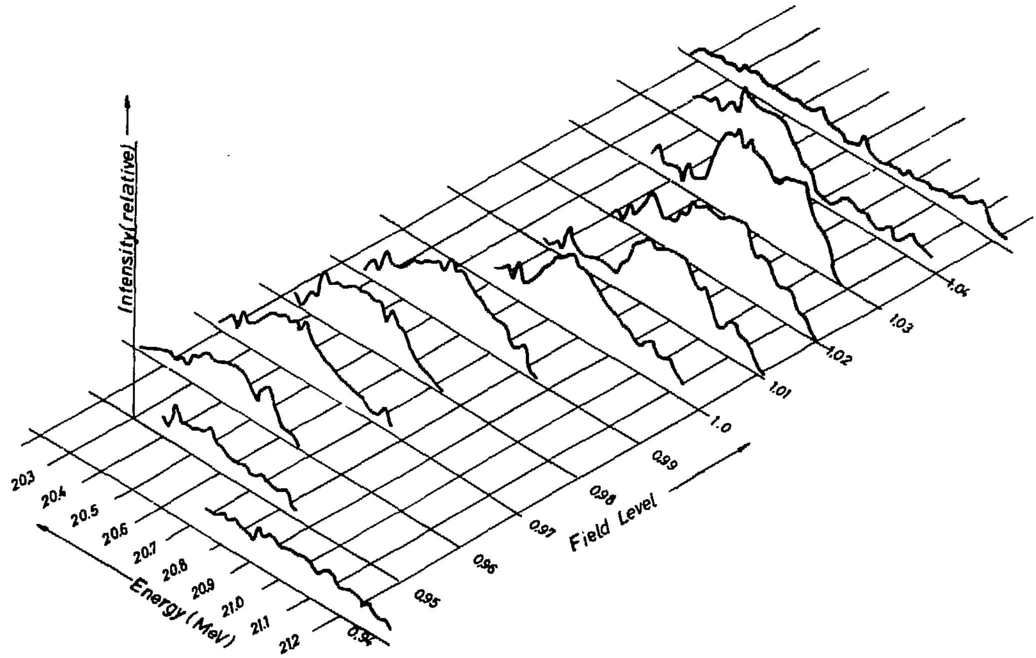

Fig.19 Measured Energy Spectrum

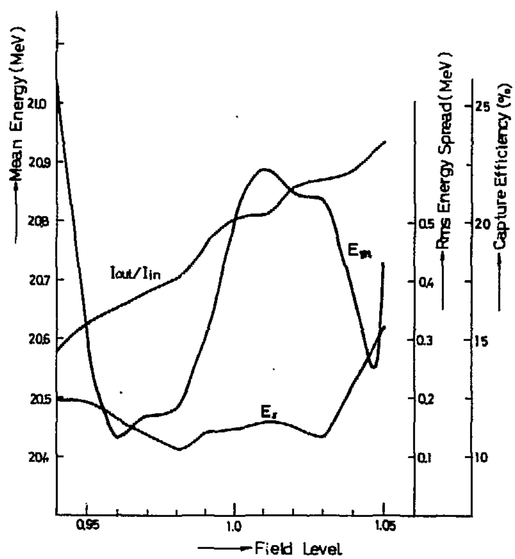

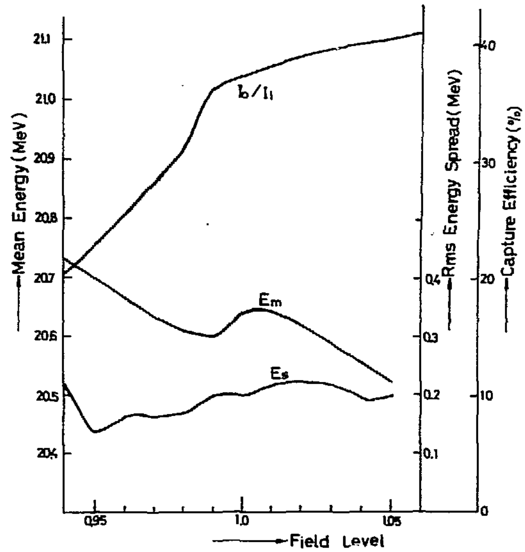

Fig.20 Experimental (left) and Computational (right) Rms Energy Spread, Mean Energy and Normalized Transmitted Current

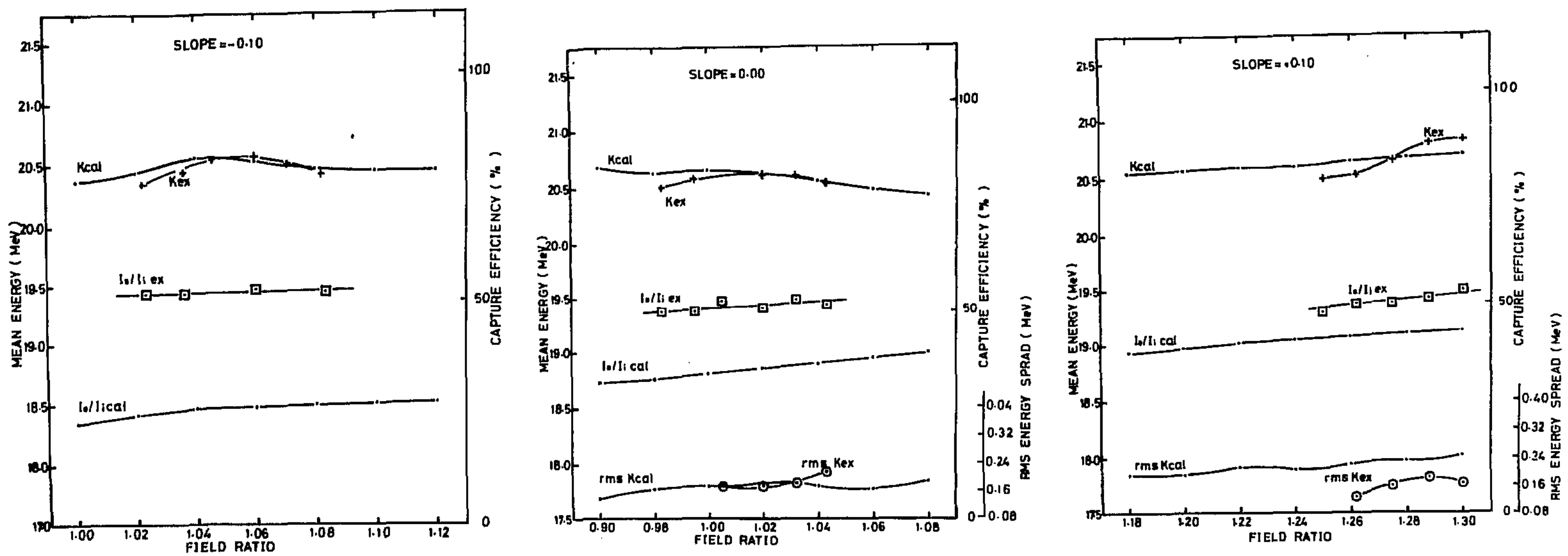

Fig.21 Experimental Mean Energy, Rms Energy Spread and Capture Efficiency at 100 mA